

# *Electronics Letters*

## Special issue Call for Papers

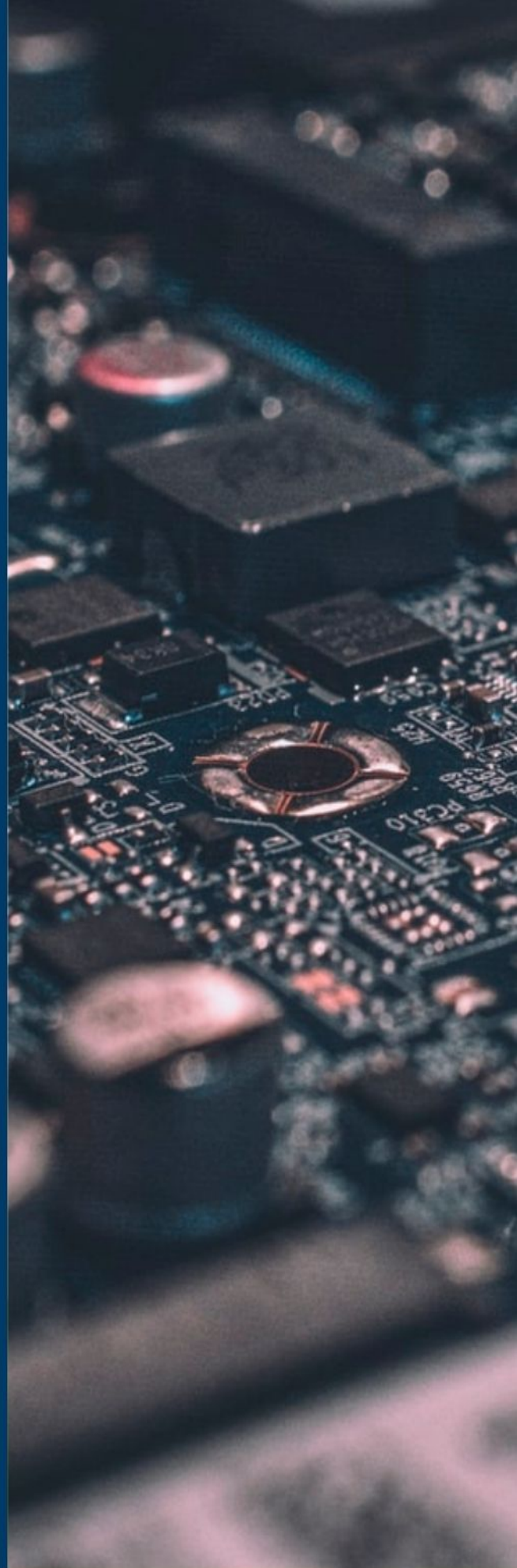
---

**Be Seen. Be Cited.  
Submit your work to a new  
IET special issue**

Connect with researchers and experts in your field and share knowledge.



Be part of the latest research trends, faster.

[Read more](#)



The Institution of  
Engineering and Technology

# An analysis of the convergence condition for narrowband FxLMS

Hao-xiang Wen,  Huan Luo, and Sen-quan Yang   
 School of Intelligent Engineering, Shaoguan University, Shaoguan City, Guangdong Province, China

Email: sqyang@sgu.edu.cn

This letter discusses the convergence condition of the narrowband FxLMS (NFxLMS) algorithm in Z-domain. First, two new concepts about NFxLMS root locus, that is critical start point (CSP) and critical cross point (CCP), are introduced and defined. For NFxLMS with the simplest case, a special characteristic of the root locus is observed that the CCP always locates itself near the CSP in the Z plane. By exploiting this characteristic, directly solving the root locus equation is eliminated from the stability analysis, and the upper bound of the step size for NFxLMS is eventually estimated as a function of the reference frequency.

**Introduction:** The noise produced by the transformer or the rotating machines such as engines, helicopters, motors, and so forth, can be considered as periodic and deterministic noises [1]. The narrowband active noise control (NANC) system equipped with the narrowband filtered-x LMS (NFxLMS) algorithm is found to be effective in reducing such noises [2, 3]. The stability analysis of the NFxLMS, which is mainly aimed at estimating the upper bound for the step size, that is  $\mu_{max}$ , can be performed in the time domain [4–6] or in the Z-domain [7–11]. However, both analyses mentioned above have their respective limitations.

**Limitations of the time domain analysis:** In the time domain analysis, the input signal sometimes has to be assumed as pseudorandom signal and sometime as random signal, even the input signal is obviously deterministic. Moreover, the time domain analysis is based on several assumptions [4–6], that is the slow adaptation assumption and the independence assumption, which would not hold when the input signal is periodic. In [6], Table 1, the estimation of  $\mu_{max}$  derived from the time domain analysis is about six times of the actual value. Furthermore, the estimation in [6] requires a computational expensive grid search.

**Limitations of the Z-domain analysis:** Because the reference signal of NFxLMS is usually deterministic and periodic, it is more suitable to consider the NANC system as a linear time-invariant (LTI) system and analyze its stability in Z-domain [7–11]. However, the root locus equation of NFxLMS is usually a higher degree parametric (HDP) equation. Due to the difficulty in solving an HDP equation, it is hard to extract any elegant expression for  $\mu_{max}$  from the analysis in Z-domain, even for the NFxLMS with the simplest case.

To avoid the difficulty in solving the root locus equation, a novel stability analysis of NFxLMS in Z-domain is proposed. The main contributions of this letter are listed as follows.

- (1) An important characteristic of the NFxLMS root locus is observed that the critical cross point (CCP) always locates itself near the critical start point (CSP) in the Z plane. Utilizing this characteristic, directly solving the root locus equation is eliminated from the stability analysis.
- (2) Based on the novel stability analysis, the value of  $\mu_{max}$  for the NFxLMS with the simplest case is estimated. The influence of the reference frequency on the estimation of  $\mu_{max}$  is considered.

**NFxLMS Algorithm and its transfer function:** The block diagram of a typical NFxLMS algorithm can be found in [6], Figure 1. The input and output signals of NFxLMS are respectively denoted as  $p(n)$  and  $e(n)$  where  $n$  is the time index. The NFxLMS is described by the following equations:

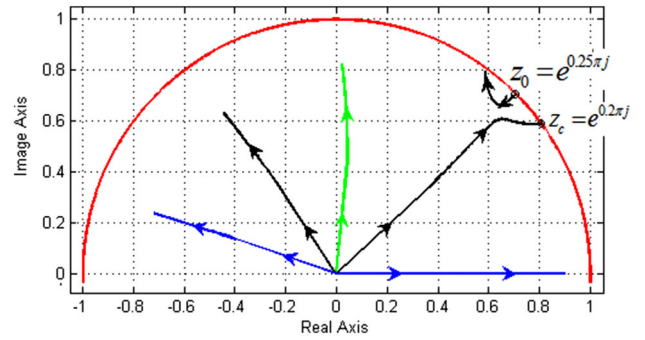


Fig. 1 The upper Z plane of NFxLMS root locus ( $\Delta = 10$  and  $\omega_0 = \pi/4$ )

$$y(n) = \sum_{i=1}^q [a_i(n) \cos(\omega_i n) + b_i(n) \sin(\omega_i n)], \quad (1a)$$

$$e(n) = p(n) - \sum_{l=0}^L s_l y(n-l), \quad (1b)$$

$$a_i(n+1) = a_i(n) + \mu e(n) \sum_{l=0}^L \hat{s}_l \cos[(n-l)\omega_i], \quad (1c)$$

$$b_i(n+1) = b_i(n) + \mu e(n) \sum_{l=0}^L \hat{s}_l \sin[(n-l)\omega_i], \quad (1d)$$

where  $\omega_i$  is the  $i$ th frequency component of the reference signal,  $q$  is the total number of the frequency components,  $s = [s_1, s_2, \dots, s_L]$  with length  $L$  is the impulse response of the secondary path (SP) and  $\hat{s} = [\hat{s}_1, \hat{s}_2, \dots, \hat{s}_L]$  is the estimation of SP, which is usually assumed to be available with the on-line or off-line system identification technique [12, 13].

The NFxLMS requires only two coefficients, that is  $a_i(n)$  and  $b_i(n)$ , to control one frequency component in the noise. The two coefficients are adapted with Equations (1c)–(1d) where  $\mu$  is the step size of the adaptation. A large  $\mu$  can increase the convergence speed. However, when  $\mu$  further increases to its upper bound  $\mu_{max}$ , the algorithm would lose its robustness [6, 9]. This letter examines the stability analysis aimed at estimating the value of  $\mu_{max}$  for the NFxLMS given by Equations (1a)–(1d).

Respectively denoting  $E(z)$ ,  $P(z)$  and  $S(z)$  as the Z transforms of  $e(n)$ ,  $p(n)$  and  $s$ , the transfer function of NFxLMS is defined as  $H(z) = E(z)/D(z)$ . After several straightforward manipulations, the transfer function of NFxLMS can be achieved from Equations (1a)–(1d) as

$$H(z) = 1 / \left( 1 + \mu S(z) \sum_{i=1}^q \frac{\alpha_i z - \beta_i}{z^2 - 2z \cos \omega_i + 1} \right) \quad (2)$$

where  $\alpha_i = \sum_{l=0}^L \hat{s}_l \cos[(l+1)\omega_i]$  and  $\beta_i = \sum_{l=0}^L \hat{s}_l \cos(l\omega_i)$ .

For the simplest case where the reference signal only has a single frequency component  $\omega_0$ , the SP is composed of a pure delay  $\Delta$ , that is  $S(z) = z^{-\Delta}$  and a perfect SP estimation is assumed, that is  $\hat{S}(z) = S(z) = z^{-\Delta}$ , (2) can be simplified as  $H(z) = (z^2 - 2z \cos \omega_0 + 1)/F(z)$ , where  $F(z)$  is given by

$$F(z) = z^2 - 2z \cos \omega_0 + 1 + \mu z^{-\Delta} [z \cos((\Delta+1)\omega_0) - \cos(\Delta\omega_0)]. \quad (3)$$

In the framework of the root locus theory, the root locus equation of NFxLMS is  $F(z) = 0$ . The  $\mu_{max}$  for NFxLMS can be estimated by searching for the maximum  $\mu$  to ensure that all the roots of  $F(z) = 0$  are inside the unit circle in Z plane [9]. From (3), the value of  $\mu_{max}(\omega_0)$  should be a function of the reference frequency  $\omega_0$ . However, due to the unsolved problem in mathematics of determining all the roots of a HDP equation, it is impossible to extract any global conclusion for  $\mu_{max}$  by directly solving  $F(z) = 0$ , even for NFxLMS with the simplest case. Only the values of  $\mu_{max}(\omega_0)$  for some particular cases, that is  $\mu_{max}(\omega_0 = 0)$  [9] and  $\mu_{max}(\omega_0 = \pi/2)$  [10, 11], have been discussed.

Table 1. Mean deviation of the estimation  $\mu_{max}$

	$\Delta = 10$	$\Delta = 20$	$\Delta = 40$	$\Delta = 60$
MD	22.8%	16.0%	11.0%	9.0%

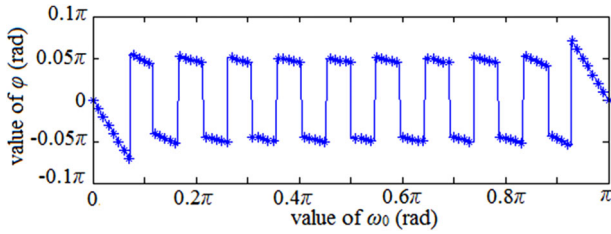


**Fig. 2** Relationship between  $\varphi$  and  $\omega_0$  ( $\Delta = 10$  and  $\omega_0 = \pi/4$ )

**Characteristic of nfxlms root locus:** An example of the NFXLMS root locus is shown in Figure 1 for  $\omega_0 = 0.25\pi$  and  $\Delta = 10$  with  $\mu$  increases from 0 to  $\mu_{\max} = 0.28$ . The arrows indicate the increasing direction of  $\mu$ . Only the upper Z plane is considered in Figure 1 because the Z plane of the NFXLMS root locus is symmetric about its horizontal axis. CSP and CCP of the NFXLMS root locus are defined as follows.

**CSP:** The start points of NFXLMS root locus are defined by the roots of  $F(z) = 0$  with  $\mu = 0$ . From (3), one of the start points certainly locates itself at  $z_0 = e^{j\omega_0}$  and this point is defined as CSP.

**CCP:** As  $\mu$  increases, some roots of  $F(z) = 0$  may cross the unit circle. The location where the first root crosses the unit circle is defined as CCP. The CCP is denoted as  $z_c = e^{j\theta}$  where  $\theta$  is the argument of  $z_c$ .

It is obvious that the value of  $\mu$  corresponding to  $z_c = e^{j\theta}$  is  $\mu_{\max}$ . If the value of  $\theta$  can be achieved, then inserting  $z_c = e^{j\theta}$  into (3) and forcing  $F(z) = 0$ , the value of  $\mu_{\max}$  can be estimated as a function of  $\omega_0$  and  $\Delta$ , as

$$\hat{\mu}_{\max}(\omega_0, \Delta) = \frac{(2z_c \cos \omega_0 - z_c^2 - 1)z_c^\Delta}{z_c \cos((\Delta + 1)\omega_0) - \cos(\Delta\omega_0)}. \quad (4)$$

In Figure 1, the CSP locates itself in  $z_0 = e^{0.25\pi j}$ . The CCP approximately locates itself in  $z_c = e^{0.2\pi j}$ , that is  $\theta = 0.2\pi$ . The CCP is in the neighbourhood of the CSP in the Z plane. To further discuss the location relationship between CCP and CSP, the argument difference between CCP  $z_c = e^{j\theta}$  and CSP  $z_0 = e^{j\omega_0}$  is introduced, which is defined as  $\varphi = \theta - \omega_0$ . The value of  $\varphi$  depends on  $\omega_0$ , and their relationship is plotted in Figure 2. From Figures 1 and 2, an important characteristic of the NFXLMS root locus is observed that the CCP always locates itself close to the CSP, that is  $0 \approx |\varphi/\pi| \ll 1$ . This characteristic will be further verified by the simulation later.

For a sufficiently small  $\varphi$ , the following approximations hold.

$$\cos(\varphi + \varphi\Delta) \approx \cos(\varphi\Delta) \text{ and } \sin(\varphi + \varphi\Delta) \approx \sin(\varphi\Delta). \quad (5)$$

#### Stability analysis of NFXLMS

Because  $\mu_{\max}$  in (4) is a real number instead of a complex number, taking real part of the numerator and denominator on left hand side of (4) leads to

$$\begin{aligned} \mu_{\max} &= f_r(\omega_0, \Delta, \theta) \\ &= \frac{2 \cos \theta (\cos \omega_0 - \cos \theta)}{\cos(\omega_0(\Delta + 1)) \cos(\theta(1 - \Delta)) - \cos(\omega_0\Delta) \cos(\theta\Delta)}, \end{aligned} \quad (6)$$

and taking image part of the numerator and denominator on left hand side of (4) leads to

$$\begin{aligned} \mu_{\max} &= f_i(\omega_0, \Delta, \theta) \\ &= \frac{2 \sin \theta (\cos \omega_0 - \cos \theta)}{\cos(\omega_0(\Delta + 1)) \sin(\theta(1 - \Delta)) + \cos(\omega_0\Delta) \sin(\theta\Delta)}. \end{aligned} \quad (7)$$

When  $\cos \omega_0 \neq \cos \theta$ , the Equation (6) = (7) leads to

$$\cos(\omega_0\Delta) \sin(\theta(\Delta + 1)) = \cos(\omega_0(\Delta + 1)) \sin(\theta\Delta). \quad (8)$$

Inserting  $\theta = \varphi + \omega_0$  into (8) and considering the approximations given in (5), (8) can be rewritten as

$$\begin{aligned} &\cos(\omega_0\Delta) [\sin(\omega_0(\Delta + 1)) \cos(\varphi\Delta) + \sin(\varphi\Delta) \cos(\omega_0(\Delta + 1))] \\ &= \cos(\omega_0(\Delta + 1)) [\sin(\omega_0\Delta) \cos(\varphi\Delta) + \sin(\varphi\Delta) \cos(\omega_0\Delta)] \end{aligned} \quad (9)$$

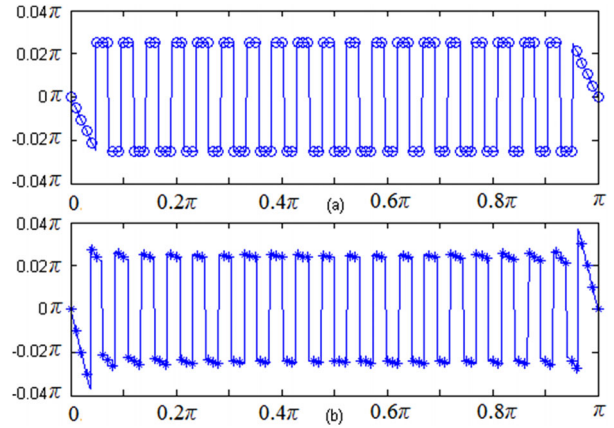


**Fig. 3** The estimated value (circles) shown in (a) and the actual value (asterisks) shown in (b) as a function of the reference frequency  $\omega_0$

Then, (9) further results in

$$\cos(\varphi\Delta) \sin(\omega_0) = 0. \quad (10)$$

When  $\omega_0 \neq k\pi$  where  $k$  is an arbitrary integer, the solution for (10) is  $\varphi\Delta = 2k\pi \pm \pi/2$ . As the value of  $\varphi$  is sufficiently small,  $\varphi$  can be estimated as

$$\varphi = -\pi/(2\Delta) \text{ or } \varphi = \pi/(2\Delta). \quad (11)$$

Equation (11) holds only when  $\omega_0 \neq k\pi$ . When  $\omega_0 \approx k\pi$ , that is  $\omega_0 \approx \pi$  or  $\omega_0 \approx 0$ , the value of  $\varphi$  cannot be estimated by any derivation. Fortunately, from Figure 2, when  $\omega_0 < \pi/(\Delta + 1)$  or  $\pi\Delta/(\Delta + 1) < \omega_0$ , a linear relationship between  $\varphi$  and  $\omega_0$  can be assumed. Moreover, from Figure 2, when  $\pi/(\Delta + 1) < \omega_0 < \pi\Delta/(\Delta + 1)$ ,  $\varphi$  seems to be a periodic function. From the information contained in Figure 2 and Equation (11), a more precise estimation of  $\varphi$  can be achieved as a function of  $\omega_0$ , as

$$\varphi(\omega_0) = \begin{cases} -\frac{\omega_0(\Delta+1)}{2\Delta}, & 0 \leq \omega_0 \leq \frac{\pi}{\Delta+1}; \\ \frac{\pi}{2\Delta}, & \frac{k\pi}{\Delta+1} < \omega_0 \leq \frac{(k+0.5)\pi}{\Delta+1}; \\ -\frac{\pi}{2\Delta}, & \frac{(k+0.5)\pi}{\Delta+1} < \omega_0 < \frac{(k+1)\pi}{\Delta+1}; \\ -\frac{(\omega_0-\pi)(\Delta+1)}{2\Delta}, & \frac{\pi\Delta}{\Delta+1} \leq \omega_0 \leq \pi; \end{cases} \quad (12)$$

where  $k$  is an integer chosen from 1 to  $\Delta + 1$ . The argument  $\theta$  of CCP, that is  $z_c = e^{j\theta}$ , can be estimated as

$$\theta = \varphi(\omega_0) + \omega_0. \quad (13)$$

Inserting  $z = e^{j\theta}$  into (4), the estimation of  $\mu_{\max}$  is achieved as

$$\hat{\mu}_{\max}(\Delta, \omega_0) = \text{Re} \left( \frac{(2z_c \cos \omega_0 - z_c^2 - 1)z_c^\Delta}{(z_c \cos((\Delta + 1)\omega_0) - \cos(\Delta\omega_0))} \right) = \frac{\text{num}}{\text{den}} \quad (14)$$

where

$$\begin{aligned} \text{den} &= [\cos(\Delta\omega_0) + \cos((\Delta + 1)\omega_0)]^2 \\ &\quad - 4\cos^2(\theta/2) \cos(\Delta\omega_0) \cos((\Delta + 1)\omega_0) \end{aligned} \quad (15)$$

$$\begin{aligned} \text{num} &= \cos(\Delta\omega_0) [\cos((\Delta + 2)\theta) + \cos(\Delta\theta)] \\ &\quad - \cos((\Delta + 1)\omega_0) [\cos((\Delta - 1)\theta) + \cos((\Delta + 1)\theta)] \\ &\quad + 2 \cos \omega_0 [\cos((\Delta + 1)\omega_0) \cos(\Delta\theta) - \cos(\Delta\omega_0) \cos((\Delta + 1)\theta)] \end{aligned} \quad (16)$$

To sum up, the estimation of  $\mu_{\max}(\Delta, \omega_0)$  for NFXLMS with the simplest case consists of the relations in the following order, (12), (13), (15), (16) and (14).

**Simulation results:** The estimation of  $\varphi(\omega_0)$  given in (12) is verified first in Figure 3. The actual value of  $\varphi$  is achieved by a search process described as follows. The  $\mu$  in (3) increases from 0 to a larger value with interval 0.001, and for each value of  $\mu$ , the equation  $F(z) = 0$  is solved



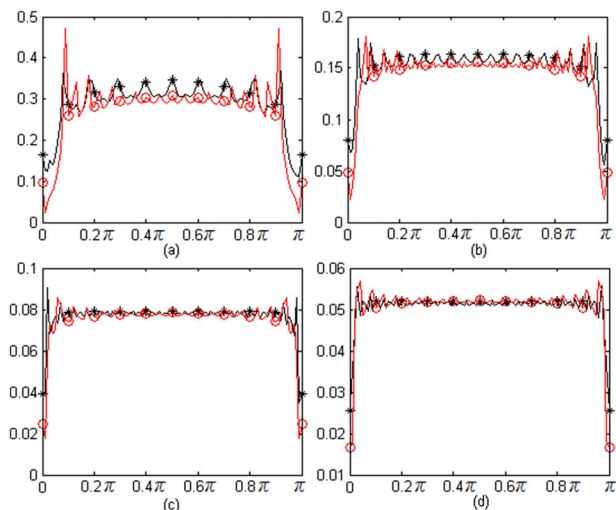


**Fig. 4** The actual value of  $\mu_{\max}$  (asterisks) and the estimated value of  $\mu_{\max}$  (circles) as a function of  $\omega_0$ . (a)  $\Delta = 10$ ; (b)  $\Delta = 20$ ; (c)  $\Delta = 40$ ; (d)  $\Delta = 60$

numerically by using the function *roots* in MATLAB. When the first root  $z_c$  crosses the unit circle, the search process stops and the actual value of  $\varphi(\omega_0)$  is achieved. The estimated value of  $\varphi(\omega_0)$  is compared with its actual value in different frequencies set as  $\omega_0 = i\pi/100$  [9] where  $i$  is an integer ranging from 0 to 100. The comparison results are shown in Figure 3 with  $\Delta = 20$ .

There are three pieces of relevant information contained in Figure 3. (1) From Figure 3, the Equation (12) performs well in predicting the value of  $\varphi(\omega_0)$  for all the reference frequencies. (2) From Equation (11), the maximum magnitude of  $\varphi(\omega_0)$  is inversely proportional to the value of  $\Delta$ . In Figure 2, the maximum magnitude of  $\varphi(\omega_0)$  with  $\Delta = 10$  is about  $0.05\pi$  and in Figure 3, the maximum magnitude of  $\varphi(\omega_0)$  with  $\Delta = 20$  is about  $0.025\pi$ . The information contained in Figures 2 and 3 verifies the inverse relationship between the magnitude of  $\varphi(\omega_0)$  and the value of  $\Delta$ . (3) From Equation (11), the magnitude of  $\varphi(\omega_0)$  becomes smaller as the value of  $\Delta$  increases. At least for  $\Delta > 10$ , the magnitude value of  $\varphi(\omega_0)$  is so small that the approximation given in (5) is reasonable.

The estimation of  $\mu_{\max}$  given by Equation (14) is verified in Figure 4. The actual value of  $\mu_{\max}$  is achieved by testing the convergence of NFxLMS given by Equations (1a)–(1d). The  $\mu$  in (1a)–(1d) increases from 0 to a larger value with interval 0.001. When the NFxLMS becomes unstable, the  $\mu$  is considered as the actual value of  $\mu_{\max}$ . The comparison results are shown in Figure 4 with different values of  $\Delta$ .

From Figure 4, only some slight deviations occur in the high and low frequency bands. In the medium frequency band, Equation (14) performs quite well in predicting the value of  $\mu_{\max}$ .

The overall precision of the estimation is evaluated by the mean deviation (*MD*), which is defined as

$$MD = \sqrt{\frac{\sum_{i=0}^{100} E^2\left(\frac{i}{100}\pi\right)}{101}}$$

$$\text{where } E(\omega_0) = \frac{\hat{\mu}_{\max}(\omega_0) - \mu_{\max}(\omega_0)}{\mu_{\max}(\omega_0)} \times 100\%. \quad (17)$$

The value of *MD* with different values of  $\Delta$  is shown in Table 1. From Table 1, the precision of the estimation improves significantly as  $\Delta$  increases. When  $\Delta > 20$ , the estimation begins to achieve a high overall precision.

**Conclusion:** To obtain a more reliable estimation of  $\mu_{\max}$  and to evaluate the influence of  $\omega_0$  on the estimation  $\mu_{\max}$ , the stability of NFxLMS with the simplest case is analyzed in Z-domain. First, an important characteristic of the NFxLMS root locus is observed that the CSP always locates itself close to the CCP in the Z plane. Then, exploiting this characteristic, directly solving the HDP equation  $F(z) = 0$  is eliminated from the convergence analysis. Finally, based on the new convergence analysis, the estimation of  $\mu_{\max}(\omega_0)$  for NFxLMS is achieved as a function of  $\omega_0$ .

However, our analysis is limited to the NFxLMS with single frequency component. The possibility of extending this analysis to the NFxLMS with multiple frequency components requires further discussion.

**Conflict of interest:** The authors declare no conflict of interest.

**Funding information:** This work was supported by National Natural Science Foundation of China with Grant/Award number 5200245

**Data availability statement:** The data that support the findings of this study are available from the corresponding author upon reasonable request.

**Credit statement:** **Hao-xiang Wen:** conceptualization; data curation; formal analysis; funding acquisition; investigation; software; writing – original draft and writing – review and editing. **Huan Luo:** software; validation; visualization; writing – original draft and writing – review and editing. **Sen-quan Yang:** validation; visualization; writing – review and editing.

© 2021 The Authors. *Electronics Letters* published by John Wiley & Sons Ltd on behalf of The Institution of Engineering and Technology

This is an open access article under the terms of the Creative Commons Attribution-NonCommercial-NoDerivs License, which permits use and distribution in any medium, provided the original work is properly cited, the use is non-commercial and no modifications or adaptations are made. Received: 20 October 2021 Accepted: 10 November 2021 doi: 10.1049/ell2.12378

## References

- Ma, Y., Xiao, Y.: A new strategy for online secondary-path modeling of narrowband active noise control. *IEEE Trans. Audio, Speech, Lang. Process.* **25**(2), 420-434 (2017)
- Bai, T., Wang, Z. & Xiao, Y. et al.: A multi-channel narrowband active noise control system with simultaneous online secondary- and feedback-path modeling. The IEEE Asia Pacific Conference of Circuits and Systems (APCCAS) 2019 was held in Bangkok, Thailand, November 11–14, (2019)
- Lopes, P.A.C., Gerald, J.A.B.: A narrowband active noise control system with reference synthesis. *Int. J. Adapt. Control Signal Process.* **33**(6), 143-152 (2019)
- Ma, Y., Xiao, Y., Ma, L., Khorasani, K.: Statistical analysis of narrowband active noise control using a simplified variable step-size FxLMS algorithm. *Signal Process.* **183**(6), 1-14 (2021)
- Zhu, W., Luo, L., Xie, A., Sun, J.: A novel FELMS-based narrowband active noise control system and its convergence analysis. *Applied Acoustic* **156**(1), 229-245 (2019)
- Xiao, Y., Ikuta, A., Ma, L., Hasegawa, K.: Stochastic analysis of the FxLMS-based narrowband active noise control system. *IEEE Trans. Audio, Speech, Lang. Process.* **16**(5), 1000-1014 (2008)
- Wang, L.V., Gan, W., Khong, A.W.H., Kuo, S.M.: Convergence analysis of narrowband feedback active noise control system with imperfect secondary path estimation. *IEEE Trans. Audio, Speech, Lang. Process.* **21**(11), 2403-2411 (2013)
- Ardekani, I.T., Abdulla, W.H.: On the stability of adaptation process in active noise control systems. *The J. Acoust. Soc. Am.* **129**(1), 173-184 (2011)
- Vicente, L., Masgrau, E.: Novel FxLMS convergence condition with deterministic reference. *IEEE Trans. Signal Process.* **54**(10), 3768-3774 (2006)
- Elliott, S.J., Stothers, I.M., Nelson, P.A.: A multiple error LMS algorithm and its application to active control of sound and vibration. *IEEE Trans. Acoust., Speech, Signal Process.* **35**(10) 1423-1434 (1987)
- Morgan, D.R., Sanford, C.: A control theory approach to the stability and transient analysis of the filtered-x LMS adaptive notch filter. *IEEE Trans. Signal Process.* **40**(9), 2341-2346 (1992)
- Chang, C., Kuo, S., Huang, C.: Secondary path modeling for narrowband active noise control systems. *Applied Acoustic* **131**(1), 154-164 (2017)
- Akhtar, M.T.: Narrowband feedback active noise control systems with secondary path modeling using gain-controlled additive random noise. *Digital Signal Process.* **111**(1), 1-13 (2021)